Frontiers of Information Technology & Electronic Engineering
www.jzus.zju.edu.cn; engineering.cae.cn; www.springerlink.com
ISSN 2095-9184 (print); ISSN 2095-9230 (online)
E-mail: jzus@zju.edu.cn

Supplementary materials for

Ziwei WAN, Chunlin ZHOU, Haotian ZHANG, Jun WU, 2023. Development of an onsite calibration device for robot manipulators. *Front Inform Technol Electron Eng*, 24(2):217-230. https://doi.org/10.1631/FITEE.2200172

1 Online accuracy measurement and monitoring

Before the robot is put into use, the robot user would install the measuring rod at the end of the robot and move the precision ball manually into the measurement area of the measuring device. Then, the robot controller would record the joint angles and XYZ displacements. During online accuracy measurement and monitoring, a test program is inserted before each operation process, which moves the ball automatically into the device's measurement area with the previously recorded joint positions, and compares the current XYZ displacements with the previously recorded displacements. If significant deviations are detected, it means that the robot's accuracy and repeatability have been severely reduced.

2 Why are five mounting positions set on the fixture?

First, at least three noncollinear constraint points are required to achieve a robust point cloud registration and accurately identify the 6D pose vector $\boldsymbol{x}$ of the measuring device frame $\{W\}$ with respect to (w.r.t.) the robot base frame $\{0\}$. Next, the observability index (OI) of the optimal measurement configurations selected from any three of the five mounting positions on multi-position fixture is significantly lower (by about 20%) than that of the optimal configurations selected from the four mounting positions (excluding position 3), which means that setting only three mounting positions on the fixture is not enough. Finally, setting too many mounting positions (more than five) will increase the manufacturing cost and operation complexity, and its corresponding accuracy improvement is very limited. The optimal number and locations of the mounting positions on the multi-position fixture will be further studied in the future.

3 Characterizing the multi-position fixture

As shown in Fig. S1, we first marked 15 points on each of the three inner faces of the triaxial mount, and then used the Hexagon RA8520-7 measuring arm to manually collect the measurement points near these marked points. After that, we conducted a plane fitting of the point cloud obtained, verified the verticality of the three inner faces, and determined a Cartesian frame based on the three mutually perpendicular planes in PolyWorks. Then, we mounted the measuring device at different mounting positions using fast-lock mechanisms, and obtained the corresponding Cartesian frames with the same method. Based on this, the relative positions of different mounting positions were measured in PolyWorks. To guarantee high measurement accuracy, the measuring arm and MultiCal were fixed on the same aluminum base plate with several F clamps during the measurement.

4 Aligning the ball's center to the virtual datum point

There are semi-automatic and fully automatic methods to align the ball's center to the virtual datum point. The former includes a manual adjustment to move the ball into the device's measurement area and an automatic robot adjustment to accurately align the tool center point (TCP) to the constraint point based

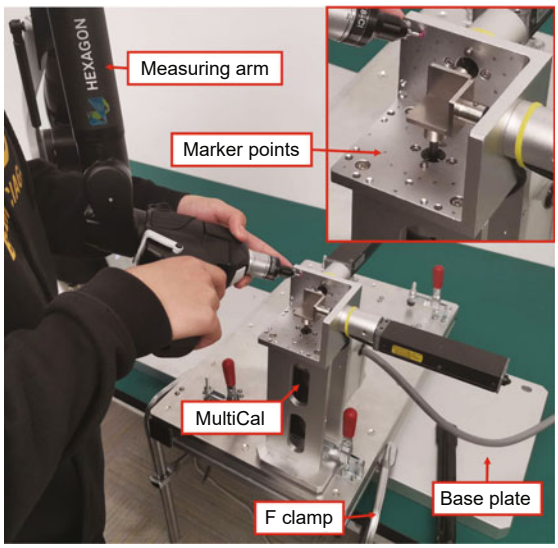

Fig. S1 Characterizing the multi-position fixture with a Hexagon measuring arm

on the feedback from the displacement sensors. The attitude angle of the robot base frame $\{0\}$ w.r.t. the measuring device frame $\{W\}$ can be determined by the ratio of the displacement feedback from different sensors, and the subsequent adjustment direction can be calculated based on this information. This method does not need to accurately establish the environment model, because the robot needs only to perform an automatic relative movement in a small space. Conversely, the fully automatic measurement is based on off-line programming (such as RoboDK), which has already been detailed in a previous work (Gaudreault et al., 2016). However, for this method, the calibration environment must be precisely modeled; otherwise, it is prone to motion collisions.

5 Optimal design of measuring rods

Apparently, the optimal parameters (l_1, l_2, and γ) of the measuring rods for different kinds of robots are different. To improve the calibration accuracy, the measuring rod should allow the robot to move in a large space, and enlarge the effect of the kinematic parameter errors of the robot's wrist joint on the final TCP errors. However, if the measuring rod is too long, the range of orientation adjustment will be insufficient, resulting in a decrease of measurement diversity. Additionally, the angle γ will affect the orientation adjustment range. To find the optimal parameters of the measuring rod for the testing robot, a variety of measuring rods with different parameters are tested in a simulation.

Typically, the measuring rod should extend to the front and side to achieve high rigidity of the rod and an appropriate range of orientation adjustment. When γ is less than 90°, it means that the measuring rod is folded inward, resulting in lower rigidity. When γ is greater than 135°, the measuring rod is close to parallel to axis 6, and will adversely affect the identification of some parameters (such as θ_5 and a_5), which will be explained below. Thus, the angle γ is set to 90° or 135° as representatives. For the case of $\gamma = 90°$, $l_1 = \{125, 200, 275, 350, 425\}$ mm, $l_2 = \{200, 275, 350, 425, 500, 575, 650\}$ mm; for the case of $\gamma = 135°$, $l_1 = \{150, 200, 250, 300, 350\}$ mm, $l_2 = \{150, 200, 250, 300, 350, 400, 450\}$ mm.

Then, different joint angle pools for robots with measuring rods of different sizes and shapes are generated. Their optimal 30 measurement configurations and the corresponding OI values are obtained with the DETMAX algorithm. Considering that the initial candidates for this algorithm have a certain impact on the final result, we randomly select the initial candidates and repeat the selection three times to obtain the optimal set of configurations with the highest OI value. The final results are used to compare the performances of different measuring rods, as presented in Fig. S2. Note that the optimal placements of the multi-position fixtures for different measuring rods are also different. Thus, we have proved, using

a simulation, that placing the multi-position fixture horizontally beside the testing robot, with the nearest distance between the fixture and robot axis 1 being about 300 to 450 mm, can achieve the highest OI value. The optimal placement height is also chosen according to the OI value through a similar simulation procedure. Normally, the optimal height of the measuring device frame $\{W\}$ w.r.t. the robot base frame $\{0\}$ is about –200 to 100 mm, and the longer the rod, the lower the fixture that needs to be placed.

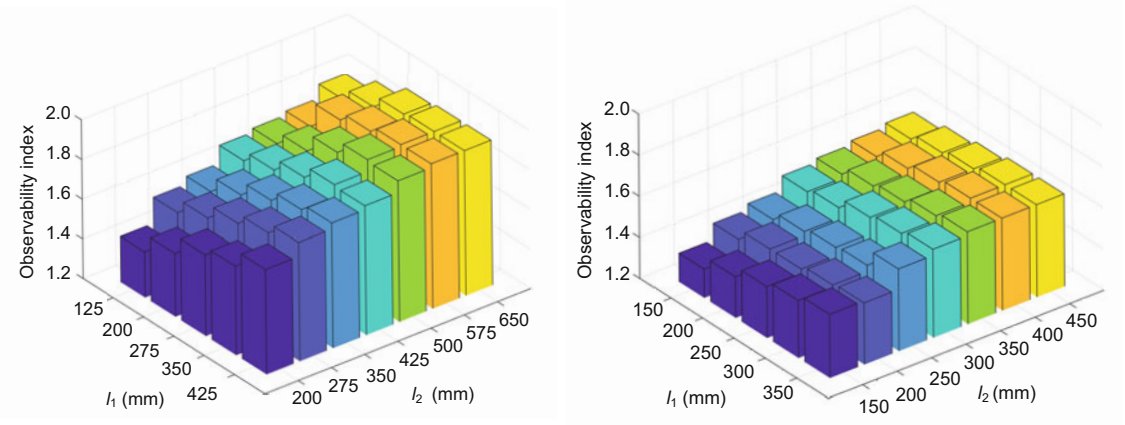

$\gamma = 90°$ $\gamma = 135°$

Fig. S2 Highest observability index (OI) values achieved by the measuring rods of different sizes and shapes in the simulation

The results show that as the length of the measuring rod increases, the OI value obtained first increases, and then gradually reaches a limit. In this trial, the highest OI value is achieved when l_1 =350 to 425 mm, l_2 =575 to 650 mm, and $\gamma = 90°$. Because the lengths of links 1–2 and 3–4 of the Staubli TX90 are both 425 mm, the theoretical optimal l_1 and l_2 are 80% to 100% and 135% to 145% of the length of the robot links respectively, and the theoretical optimal γ is 90°. Note that the measuring rod is regarded as an absolute rigid body in simulation, without considering rod deflections.

Additionally, the highest OI values achieved by the measuring rods with $\gamma = 90°$ are generally higher than those of the rods with $\gamma = 135°$. To explain this phenomenon, we analyze the correlation of each two column vectors in the identification Jacobian matrix and obtain an m-dimensional square matrix $\boldsymbol{R}$ composed of their correlation coefficients, where m is the number of parameters that need to be identified ($m = 27$ in this work), and the element $r(i, j)$ in $\boldsymbol{R}$ can be calculated as

$$r(i,j) = \frac{\mathrm{Cov}(\boldsymbol{J}_i, \boldsymbol{J}_j)}{\sqrt{\mathrm{Var}(\boldsymbol{J}_i)\,\mathrm{Var}(\boldsymbol{J}_j)}}, \tag{S1}$$

where $\boldsymbol{J}_i$ and $\boldsymbol{J}_j$ are the i^{th} and j^{th} column vectors of the Jacobian matrix, respectively. If the absolute value of $r(i, j)$ is close to 1, it means that the two kinematic parameter error terms are highly coupled and have a similar effect on the final TCP error. This will cause a degeneration of the Jacobian matrix, and ultimately reduce the OI value.

Based on this, we first set both l_1 and l_2 to 200 mm, and γ to 90° and 135° to simulate two measuring rods respectively. Then, with the same 30 measurement configurations, the above-mentioned matrix $\boldsymbol{R}$ of each measuring rod is calculated separately, and its $r(i, j)$ elements with absolute values greater than 0.85 are highlighted. Finally, the corresponding highly coupled error terms in the MDH parameters are determined, as presented in Table S1.

The results suggest that the error coupling in the case of $\gamma = 135°$ is clearly more serious than that in the case of $\gamma = 90°$. Because when γ is close to 180°, the measuring rod is approximately parallel to the axis of robot joint 6 (axis 6). At this time, both $\delta\theta_5$ and δa_5 produce an offset of the TCP perpendicular to axis 6, resulting in a strong coupling of these error terms. However, when γ is close to 90°, $\delta\theta_5$ will cause an offset

Table S1 Highly coupled error terms in MDH parameters and their correlation coefficients at different γ's

$r(i,j)$	Coupled errors	Correlation coefficient	
		$\gamma = 90^\circ$	$\gamma = 135^\circ$
$r(15,17)$	$\delta\theta_5$ & δa_5	-0.850	-0.968
$r(16,18)$	δd_5 & $\delta\alpha_5$	0.883	0.967

of the TCP in both the perpendicular and parallel directions of axis 6, which can be distinguished from the single effect of δa_5, thereby reducing the coupling of these error terms. A similar phenomenon occurs on δd_5 and $\delta\alpha_5$.

6 Simulation results

To compare MultiCal with traditional calibration methods at the theoretical level, a simulation comparison is conducted in RoboDK and MATLAB. We choose the traditional methods based on non-contact 3D measuring (3DM) devices (such as a laser tracker and a single SMR) (Sun et al., 2016), 6D measuring (6DM) devices (such as a laser tracker with a triangular artifact and three SMRs) (Nubiola et al., 2014), and 1D measuring (1DM) devices (such as a single wire draw encoder) (Zhan, 2015), and the circular point analysis (CPA) method (Cho et al., 2019) as representatives. In the trial of MultiCal, the measuring rod with l_1–l_2–γ is 125–500–90 rather than 425–650–90, attaining a higher OI value in the simulation, is chosen. This is because the latter has worse calibration performance due to rod deflection in the real environment.

First, we add 100 sets of random errors to the MDH parameters (the ranges of the length errors and the angle errors are ± 1 mm and $\pm 0.5^\circ$, respectively) to simulate 100 virtual robots. Second, the corresponding 100 sets of optimal n measurement configurations for different methods are generated. All of these configurations must be reachable, measurable, and free of collision. For MultiCal, 6DM, 3DM, and 1DM, n is 40, and the above-described observability index and DETMAX algorithm are used. For CPA, n is 60 (10 measuring points for each joint), and the motion range of each single axis is as large as possible. Then, the corresponding 100 sets of TCPs are solved using the forward kinematic equation, and the different virtual measurement outputs are generated according to the type of measuring device. Third, we add some artificial measurement noises and joint angle noises (normal distributed, and the variances are σ_1 and σ_2, respectively) to these virtual measurements, while $\sigma_1 = \{0.8, 0.4, 0.2, 0.1, 0.05, 0.025, 0.0125, 0.0063, 0.0032\}$ mm, and $\delta_2 = \{0.1, 0.05, 0.025, 0.0125, 0.0063, 0.0032\}^\circ$. For the case of 6DM, a triangular artifact and three SMRs are simulated, so the orientation measurement error e_{ori} can be approximately calculated and added to the simulated 6D measurement data using Eq. (S2):

$$e_{\text{ori}} = \arcsin\left(e_{\text{pos}}/D_{\text{SMR}}\right), \tag{S2}$$

where e_{pos} is the position measurement error of the single SMR, and D_{SMR} is the distance between every two SMRs, which is 200 mm in this work.

Finally, the 100 virtual robots are calibrated using the different simulation data and calibration methods. Then, using the ISO standard method (ISO, 1998), we virtually measure the absolute position errors of these robots without any measurement noise or joint angle noise, and obtain the mean position errors as the calibration performances of different methods (Fig. S3).

The results demonstrate that for most cases, the calibration accuracy of 6DM is only 5% to 10% better than that of 3DM, and both of them have the highest calibration accuracy with the position errors being only 36% to 42% of that of 1DM. The calibration accuracy of MultiCal is 10% to 20% lower than that of 3DM, indicating that the reduction of measurement diversity (the defect of MultiCal) has a significantly less negative effect on calibration accuracy in contrast to the dimensionality reduction of measurement data (the drawback of 1DM). Additionally, CPA is the most sensitive to measurement accuracy. If the device's accuracy is high, it has an overall appealing performance because it is not affected by the joint angle noise. However, if the device's accuracy is low, the overall performance of CPA is relatively poor. This may be

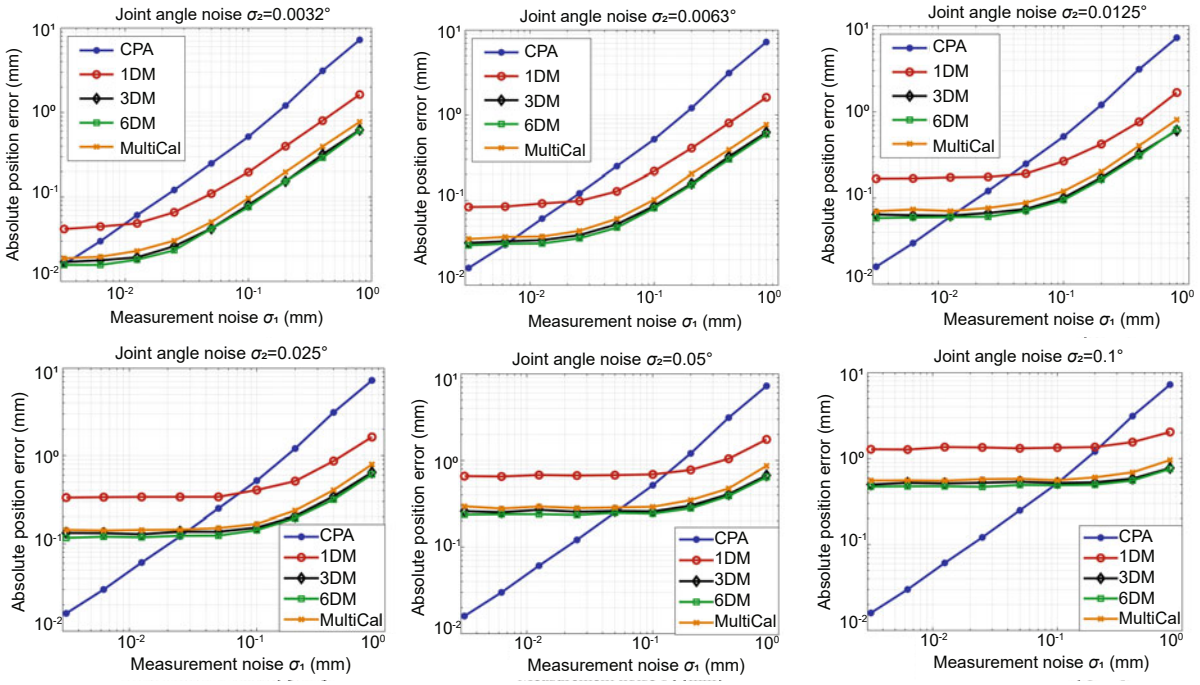

Fig. S3 Simulation comparison of MultiCal, the circular point analysis (CPA) method, and traditional calibration methods based on 6D measuring (6DM), 3D measuring (3DM), and 1D measuring (1DM) devices with different measurement noises (σ_1) and joint angle noises (σ_2)

because the MDH parameters are very sensitive to the identification errors of the joint axes, which will increase drastically as the device's accuracy decreases. Because the accuracy of measuring devices (often worse than 0.05 mm) is generally worse than that of joint encoders (often better than 0.01°), CPA would have the worst performance in actual calibration. Except for CPA, as the device's accuracy increases, the calibration accuracies of the other methods gradually reach their limits, which are determined by the joint angle error.

References

Cho Y, Do HM, Cheong J, 2019. Screw based kinematic calibration method for robot manipulators with joint compliance using circular point analysis. *Robot Comput-Integr Manuf*, 60:63-76. https://doi.org/10.1016/j.rcim.2018.08.001

Gaudreault M, Joubair A, Bonev IA, 2016. Local and closed-loop calibration of an industrial serial robot using a new low-cost 3D measuring device. IEEE Int Conf on Robotics and Automation, p.4312-4319. https://doi.org/10.1109/ICRA.2016.7487629

ISO, 1998. Manipulating Industrial Robots—Performance Criteria and Related Test Methods. ISO 9283:1998. International Organization of Standards.

Nubiola A, Slamani M, Joubair A, et al., 2014. Comparison of two calibration methods for a small industrial robot based on an optical CMM and a laser tracker. *Robotica*, 32(3):447-466. https://doi.org/10.1017/S0263574713000714

Sun T, Zhai Y, Song Y, et al., 2016. Kinematic calibration of a 3-DoF rotational parallel manipulator using laser tracker. *Robot Comput-Integr Manuf*, 41:78-91. https://doi.org/10.1016/j.rcim.2016.02.008

Zhan Y, 2015. Development of a Wire Draw Encoder Based Measurement System for Robot Calibration. MS Thesis, the Hong Kong University of Science and Technology, Hong Kong, China.